sustainability

MDPI

Article

Experimental Study on the Properties of Basalt Fiber–Cement-Stabilized Expansive Soil

Junhua Chen [1,2], Jiejie Mu [1], Aijun Chen [1,*], Yao Long [3,*], Yanjiang Zhang [1] and Jinfeng Zou [2]

[1] School of Architecture and Transportation Engineering, Guilin University of Electronic Technology, Guilin 541004, China; jhchan@126.com (J.C.); mjj526105@gmail.com (J.M.); yanjiangzhang@163.com (Y.Z.)
[2] School of Civil Engineering, Central South University, Changsha 410075, China; zoujinfneg_0@163.com
[3] School of Railway Engineering, Hunan Technical College of Railway High-Speed, Hengyang 421002, China
* Correspondence: caj3026@guet.edu.cn (A.C.); ly_dylan@163.com (Y.L.)

Abstract: Expansive soil is prone to rapid strength degradation caused by repeated volume swelling and shrinkage under alternating dry–wet conditions. Basalt fiber (BF) and cement are utilized to stabilize expansive soil, aiming to curb its swelling and shrinkage, enhance its strength, and ensure its durability in dry–wet cycles. This study examines the impact of varying content (0–1%) of BF on the physical and mechanical characteristics of expansive soil stabilized with a 6% cement content. We investigated these effects through a series of experiments including compaction, swelling and shrinkage, unconfined compressive strength (UCS), undrained and consolidation shear, dry–wet cycles, and scanning electron microscope (SEM) analyses. The experiments yielded the following conclusions: Combining cement and BF to stabilize expansive soil leverages cement's chemical curing ability and BF's reinforcing effect. Incorporating 0.4% BFs significantly improves the swelling and shrinkage characteristics of cement-stabilized expansive soils, reducing expansion by 36.17% and contraction by 28.4%. Furthermore, it enhances both the initial strength and durability of these soils under dry–wet cycles. Without dry–wet cycles, the addition of 0.4% BFs increased UCS by 24.8% and shear strength by 24.6% to 40%. After 16 dry–wet cycles, the UCS improved by 38.87% compared to cement-stabilized expansive soil alone. Both the content of BF and the number of dry–wet cycles significantly influenced the UCS of cement-stabilized expansive soils. Multivariate nonlinear equations were used to model the UCS, offering a predictive framework for assessing the strength of these soils under varying BF contents and dry–wet cycles. The cement hydrate adheres to the fiber surface, increasing adhesion and friction between the fibers and soil particles. Additionally, the fibers form a network structure within the soil. These factors collectively enhance the strength, deformation resistance, and durability of cement-stabilized expansive soils. These findings offer valuable insights into combining traditional cementitious materials with basalt fiber to manage expansive soil hazards, reduce resource consumption, and mitigate environmental impacts, thereby contributing to sustainable development.

Keywords: basalt fiber; expansive soil; swelling and shrinkage; shear strength; unconfined compressive strength; dry–wet cycles

Citation: Chen, J.; Mu, J.; Chen, A.; Long, Y.; Zhang, Y.; Zou, J. Experimental Study on the Properties of Basalt Fiber–Cement-Stabilized Expansive Soil. *Sustainability* **2024**, *16*, 7579. https://doi.org/10.3390/su16177579

Academic Editor: Anna De Marco

Received: 11 June 2024
Revised: 5 July 2024
Accepted: 16 July 2024
Published: 1 September 2024

1. Introduction

Expansive soil contains high concentrations of expansive clay minerals like montmorillonite, illite, and kaolinite. When subjected to alternating wet and dry conditions, expansive soil experiences significant volume changes, including swelling and shrinkage, leading to rapid strength degradation. This poses a severe risk to shallow, lightweight structures such as highway projects [1–3]. Highway projects constructed in expansive soil regions frequently encounter slope landslides, roadbed deformations, structural damage, etc. The repetitive and prolonged nature of these damages results in substantial losses to engineering and construction endeavors [4–6]. Therefore, stabilizing expansive soil

becomes imperative to mitigating its expansive and contractive tendencies while enhancing its resistance to dry–wet cycles [7].

Traditional chemical modification techniques such as cement and lime offer ease of construction and high soil stabilization strength, making them widely utilized in various road engineering projects [7–9]. However, the production process of cement, lime, and other stabilizing agents entails significant natural resource consumption and emits greenhouse gases like carbon dioxide. Moreover, soil stabilized with cement and other curing agents is prone to brittle damage [8]. Consequently, many scholars have proposed a physical stabilization method involving fiber reinforcement. This approach entails adding various fibrous materials to soil to enhance the engineering properties of expansive soil. Festugato et al. [10] and Yang et al. [11] investigated the effects of different fiber lengths, incorporation methods, and curing times on the compressive, tensile, and splitting strengths of fiber–cement composites for stabilized soil, respectively. They discovered that fibers effectively increased soil strength and hindered crack development. Wasim M. T. et al. [12] introduced three different jute fibers to expansive soil and observed increased shear strength and CBR values through mechanical tests. The experimental results further demonstrated the micro-level bonding effect between fiber and soil particles. Pourakbar S. et al. [13] evaluated the effect of incorporating wollastonite microfibers into soils through UCS, indirect tensile strength (ITS), and flexural strength (FS) tests. The results showed that incorporating fibers improved both the peak and post-peak responses in the UCS, ITS, and FS tests. Kanchi M. G. et al. [14] developed an analytical model for fiber-reinforced soil based on the modified Cambridge model, investigating in detail the effect of fiber orientation on the soil's stress–strain characteristics. The results showed that fibers had the greatest effect in the extension direction. The contribution of fibers to the strength of fiber-reinforced soil decreases as the angle of inclination of the fibers to the horizontal increases. These studies collectively demonstrated that the physical and mechanical properties of expansive soil can be enhanced through chemical or physical amendments.

Nonetheless, this study highlights that the mechanical properties of expansive soil, even when enhanced with traditional hydraulic materials, experience considerable deterioration under repeated dry–wet cycles [15–17]. Consequently, researchers have sought to enhance expansive soil through various chemical reinforcements and fibers. Zhang et al. [18] investigated the compression and shear properties of OPC-MCA and basalt fiber-stabilized shield waste sludge after dry–wet cycles, noting that the addition of basalt fiber improved resistance to such cycles. Shu et al. [19] examined the mechanical properties of salt-affected soil co-cured with sulfur-free lignin, basalt fiber, and hydrophobic polymers, observing heightened resistance to degradation from dry–wet cycles. Nguyen L. et al. [20] conducted a series of undrained triaxial tests on natural Ballina clay treated with cement and 0.3% to 0.5% fibers. The results showed that the peak shear strength of the cement- and fiber-treated soft clay increased significantly due to the formation of cement bonds and the bridging effect provided by the fibers. Additionally, the brittleness caused by cement bond breakage was significantly reduced due to fiber incorporation. Basalt fiber (BF), produced by melting basalt ore at high temperatures and forming it into a wire, offers environmental safety. Compared to other fibers, BF possesses not only a high modulus of elasticity and tensile strength, but also favorable tensile properties and chemical stability [21,22]. Leveraging the exceptional curing capabilities of cement, BF holds promise for further enhancing the engineering performance of expansive soil, reducing construction costs, and minimizing environmental impact, thereby promoting sustainable development. While BF is predominantly utilized to reinforce asphalt concrete or concrete pavements due to its capacity to inhibit shrinkage cracking and enhance material mechanics [23–25], its potential for strengthening fine-grained soils in road construction remains underexplored and warrants further investigation.

In this study, we investigated the physical and mechanical properties of BF–cement-stabilized expansive soil through comprehensive indoor testing, elucidating their micromechanical mechanisms via microstructural analysis. Initially, a compaction test determined

the optimal water content and maximum dry density of the stabilized expansive soil. Subsequently, the effectiveness of BF–cement stabilization was assessed through tests on swelling and shrinkage, unconfined compressive strength (UCS), and undrained and consolidation shear. The BF–cement-stabilized soil's resistance to dry and wet erosion post-fibrous reinforcement was analyzed using dry–wet cycle testing. Finally, scanning electron microscopy (SEM) was employed to examine the improvement mechanism of BF–cement-stabilized expansive soil and the evolution of its microscopic morphology during dry–wet cycles, further illuminating the microscopic deterioration mechanisms under dry–wet conditions.

2. Test Materials and Methods

2.1. Test Materials

2.1.1. Expansive Soil

Testing utilized expansive soil sourced from Nanning City, Guangxi. Representative soil samples were collected, dried, crushed, and sieved to a 2 mm size, as shown in Figure 1a. The basic physical properties were assessed in accordance with the Geotechnical Test Standard (GB/T 50123-2019) [26], with the results presented in Table 1. Referring to the Technical Specification for Construction in Expansive Soil Areas (GB50112-2013) [27] and the data in Table 1, the soil sample exhibited a free swelling rate of 51.7%. This indicates a preliminary classification of the soil as weakly expansive.

(**a**) (**b**) (**c**)

Figure 1. Test materials: (**a**) Portland cement; (**b**) Basalt fiber; (**c**) Expansive soil.

Table 1. Basic physical and mechanical parameters of expansive soil.

Maximum Dry Density (g/cm^3)	Specific Gravity	Liquid Limit/%	Plastic Limit/%	Plasticity Index	Sticky Grain Content/%	
					<0.005 mm	<0.0025 mm
1.98	2.68	54.3	24.2	30.1	55.03	53.3

2.1.2. Basalt Fiber (BF) and Cement

The basalt fiber (BF) utilized in this study was manufactured by Shanghai Chenqi Chemical Technology Co. (Shanghai, China), as shown in Figure 1b. The primary performance indicators are detailed in Table 2.

Table 2. Basic physical and mechanical parameters of basalt fiber.

BF Length (mm)	Monofilament Diameter (μm)	Densities (g/cm^3)	Modulus of Elasticity (GPa)	Tensile Strength (MPa)
6	7~15	2.64	90~110	3000~4800

The cement used, as shown in Figure 1c, was ordinary Portland cement manufactured in Xingan County, Guilin City. The key performance parameters are provided in Table 3.

Table 3. Main performance indicators of cement.

Packing Density (g/m^3)	Specific Surface Area (m^2/kg)	Solidification Time (min)		Compressive Strength (GPa)	
		Initial Condensation	Final Condensation	3 d	28 d
1.60	300	175	231	23.7	45.6

2.2. Test Methods

2.2.1. Compaction Test

According to Geotechnical Test Standard (GB/T 50123-2019) [26], the expanded soil samples underwent pulverization and sieving through a 5 mm sieve, followed by drying and storage. Subsequently, these samples were blended with cement and BF to produce five sets of specimens, each varying in moisture content by approximately 2%, and were sealed for 1 h. Compaction tests were then conducted using the heavy-duty compaction method within the subsequent 1 h, as shown in Figure 2a. The mass of each specimen was measured upon completion of compaction, as shown in Figure 2b. Finally, soil samples were extracted from the center of each specimen to ascertain their moisture content.

(**a**) (**b**)

Figure 2. Compaction test equipment and specimens: (**a**) Heavy-duty compactor and (**b**) compacted specimens.

2.2.2. Swelling and Shrinkage Test

The expanded soil was sieved through a 2 mm sieve and subsequently dried. The quantity of material was determined based on the optimal moisture content and maximum dry density obtained from the compaction test. Specimens measuring φ61.8 mm × H20 mm were compacted in three layers to achieve 95% compaction using a ring cutter, as shown in Figure 3a. These prepared specimens were sealed in plastic bags and cured for 28 d in a standard curing box, at a maintained temperature of (22 ± 2) °C and a relative humidity of 95 ± 2%. The unloaded expansion ratio and contraction ratio of the specimens were assessed using a WZ-2 Expansion Meter (Wuxi Serve Real Technology Co., Ltd., Wuxi, China) and SS-1 Shrinkage Meter (Zhejiang Tugong Instrument Co., Ltd., Shaoxing, China), as shown in Figure 3b,c.

(**a**) (**b**) (**c**)

Figure 3. Swelling and shrinkage test equipment and specimens: (**a**) Ring knife specimens; (**b**) SS-1 Shrinkage Meter; (**c**) WZ-2 Swelling Meter.

2.2.3. Unconfined Compressive Strength (UCS) Test

The specimens were statically pressed into specimens measuring φ50 mm × H100 mm using a jack, achieving 95% compaction. After demolding with an electric stripper, they were cured for 28 d. Loading was performed using a Model TSZ30-2.0 Strain Controlled Triaxial Test Apparatus (Nanjing T-Bota Scietech Instruments & Equipment Co., Ltd., Nanjing, China) at a controlled rate of 1 mm/min. To minimize testing errors, three parallel specimens were arranged for each test set. The test equipment and process are shown in Figure 4.

Figure 4. UCS test equipment and process: (**a**) Jack; (**b**) Electric stripper; (**c**) Specimens for UCS test; (**d**) Standard curing box; (**e**) Model TSZ30-2.0 Strain Controlled Triaxial Test Apparatus.

2.2.4. Undrained and Consolidation (CU) Shear Test

Triaxial shear specimens were prepared by compacting them in five layers using a three-valve saturator and a compacting hammer. The dry density of the specimens was controlled to reach 90% of the maximum dry density. The specimens were cylindrical with dimensions of φ39.1 mm × H80 mm. After 28 d of curing, the specimens were saturated using an evacuating device and then subjected to shear tests with the Model TSZ-3 Strain Controlled Triaxial Test Apparatus at a controlled shear rate of 0.08 mm/min. Peripheral pressures were controlled at 100, 200, and 300 kPa, respectively. The test equipment and process are shown in Figure 5.

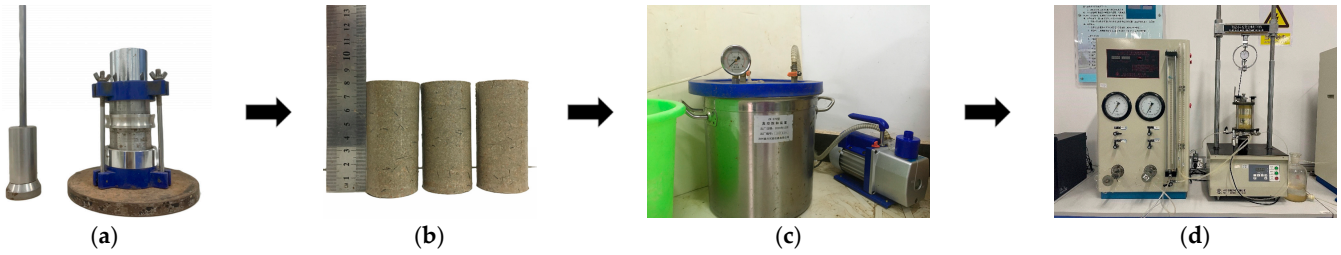

Figure 5. CU test equipment and process: (**a**) Saturator and compacting hammer; (**b**) Specimens for CU test; (**c**) Evacuating device; (**d**) Model TSZ-3 Strain Controlled Triaxial Test Apparatus.

2.2.5. Dry–Wet Cycle Test

In this study, aligned with actual engineering conditions, the duration of drying and wetting in each cycle was fixed at 12 h. The procedure involved the following.

Wetting: Initially, the specimen undergoing curing was removed and wrapped in gauze, then placed on a permeable stone. Over the first 3 h, the gauze was sprayed with a water jet every half hour to ensure thorough moistening. Subsequently, for the remaining 9 h, the gauze was moistened hourly until the humidification process was complete.

Drying: Upon completion of the wetting process, the gauze was removed from the specimen, which was then transferred to an electric blast drying oven set at 50 °C for 12 h.

This constituted a single cycle of the dry–wet procedure, as shown in Figure 6. The designated numbers of dry–wet cycles were 0, 3, 5, 7, 11, and 16. The UCS of the specimens was assessed after each dry–wet cycles.

Figure 6. Dry–wet cycle procedure.

2.2.6. Scanning Electron Microscope (SEM) Test

Several representative specimens were chosen and their bottom surfaces were smoothed with sandpaper to achieve a uniform thickness of approximately 3 mm. Any soil particles floating on the observation surface of the specimens were carefully removed using a brush. To enhance the quality and resolution of the SEM images, the samples were affixed to the sample-carrying tray using conductive adhesive and then gold-coated via vacuum spraying using a GVC-1000 ion sputterer (KYKY Technology Development Ltd., Beijing, China), as shown in Figure 7a. Subsequently, SEM testing was conducted using a KYKY-EM6200 electron microscope scanner (KYKY Technology Development Ltd., Beijing, China), as shown in Figure 7b.

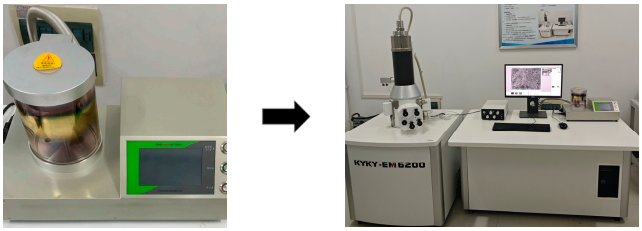

(**a**) (**b**)

Figure 7. SEM test equipment and process: (**a**) Ion Sputtering Instrument GVC-1000; (**b**) Electron Microscope Scanner KYKY-EM6200.

3. Test Results and Analyses

3.1. Compaction Property

To explore the influence of BF on the compaction characteristics of cement-stabilized expansive soil, compaction tests were conducted on specimens with varying ratios of cement to BF. The test results are depicted in Figure 8. As can be seen from the figure, the optimal water content of cement-stabilized expansive soil remained relatively consistent as the BF content increased, whereas the maximum dry density gradually decreased. However, these changes were minor overall. This phenomenon may be attributed to the similarity in density between BF and expansive soil, coupled with the relatively low BF content. Additionally, the elastic properties of BF enable it to absorb some compaction energy, rendering the mixture challenging to compact [25].

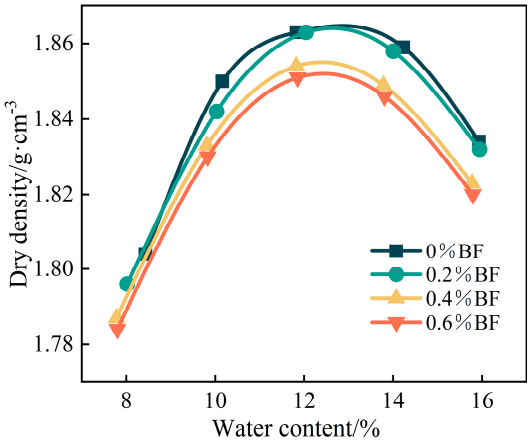

Figure 8. Compaction curves of cement-stabilized expansive soil at different BF contents.

3.2. Swelling and Shrinkage Property

3.2.1. No Loading–Swelling Ratio

Figure 9 illustrates the swelling ratio–time curves of the cement-stabilized expansive soil under no loading conditions at various BF contents. It is evident from the figure that all swelling ratios exhibited a rapid increase followed by stabilization over time. The addition of BF proved beneficial in further mitigating the swelling tendency of cement-stabilized expansive soil. Over the same duration, swelling ratios initially declined and then rose with increasing BF content. This behavior is attributed to BF's ability to inhibit specimen swelling and deformation during immersion and swelling, counteracting internal swelling forces [12]. Increasing the BF content from 0% to 0.4% reduced the swelling ratio of the cement-stabilized expansive soil from 0.33% to 0.21%, marking a 36.17% reduction compared to soil without BF. However, at 0.6% BF content, the inhibitory effect on soil swelling and deformation weakened. This indicates that higher BF incorporation does not necessarily enhance the suppression of soil swelling properties. Hence, increased incorporation of BF does not necessarily enhance the effectiveness of suppressing the soil's swelling property.

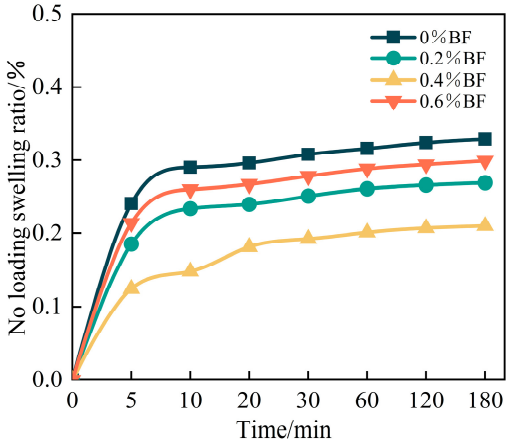

Figure 9. No loading–swelling ratio–time curves of cement-stabilized expansive soil at different BF contents.

3.2.2. Shrinkage Ratio

Figure 10 illustrates the variation curves of the shrinkage ratio of the cement-stabilized expansive soil with different amounts of BF added over 48 h. It is evident from the figure that the shrinkage ratio of all specimens exhibited a negative correlation with moisture content. The incorporation of BF yielded a mitigating effect on the shrinkage of expansive

soil. Specifically, at equivalent moisture content, the shrinkage of the BF–cement-stabilized expansive soil demonstrated a trend of initially decreasing and then increasing. At a BF content of 0.4%, shrinkage reached 5.8% in the dry state, indicating a reduction of 28.4% compared to cement-stabilized expansive soil alone. These findings underscore the beneficial impact of BF in further reducing the shrinkage of cement-stabilized expansive soil.

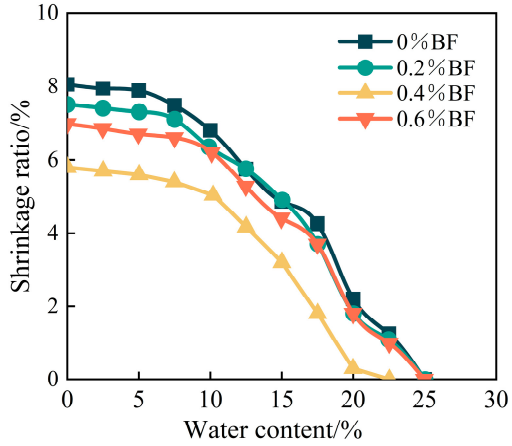

Figure 10. Shrinkage variation curves of cement-stabilized expansive soil at different BF contents.

3.3. Mechanical Properties

3.3.1. Unconfined Compressive Strength (UCS)

The UCS test evaluated the compressive properties of cement-stabilized expansive soil when varying amounts of BF were added. This test was crucial for determining how BF content affected the mechanical strength of the soil. The UCS of the cement-stabilized expansive soil at various BF contents is illustrated in Figure 11. It is evident from the figure that BF content significantly influenced the compressive properties of cement-stabilized expansive soil. Specifically, the UCS of cement-stabilized expansive soil exhibited a trend of initially increasing and then decreasing with rising BF content. The peak UCS value was attained at a BF content of 0.4%. This increase in compressive strength amounted to 24.8% compared to cement-stabilized expansive soil without BF addition. However, with a further increase in BF content to 0.6%, the UCS diminished by 117.4 kPa. This observation serves as a pertinent example highlighting the limitations of continuously escalating BF content to enhance strength.

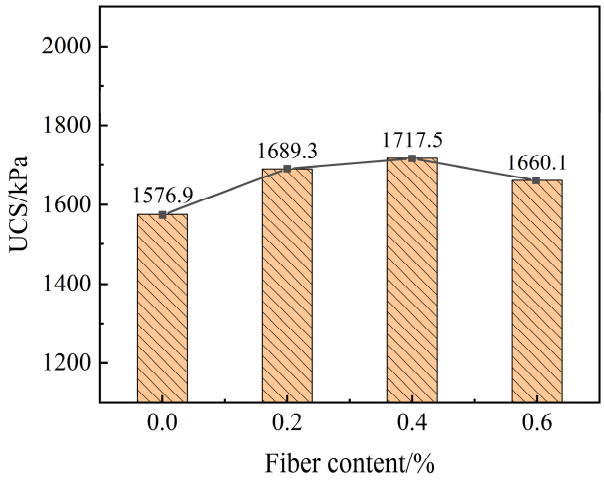

Figure 11. UCS of cement-stabilized expansive soil at different BF contents.

3.3.2. Partial Stress–Strain Curve

A partial stress–strain curve was used to analyze the behavior of the cement-stabilized expansive soil with varying BF contents under different perimeter pressures. This test helps in understanding soil's strain-softening characteristics and its response to different pressure levels. Figure 12 illustrates the partial stress–strain curves of the cement-stabilized expansive soil at varying contents of BF under different perimeter pressures. As depicted in Figure 7, the partial stress–strain curve of the cement-stabilized expansive soil without added BF exhibits typical strain-softening characteristics. Initially, its partial stress ascends to a peak and subsequently declines with increasing strain. Notably, when the perimeter pressure fell below 200 kPa, the partial stress of cement-stabilized expansive soil reached a peak before sharply dropping, indicating significant brittle damage to the soil. The data indicate that cement enhanced the overall strength of the expansive soil. However, it also rendered the damage pattern of the specimen akin to cement–concrete-type materials. At a perimeter pressure of 300 kPa, the decreasing trend of partial stress in cement-stabilized expansive soil post-peak value diminished. This finding demonstrates that appropriately increasing the perimeter pressure can mitigate the occurrence of brittle damage in cement-stabilized expansive soil.

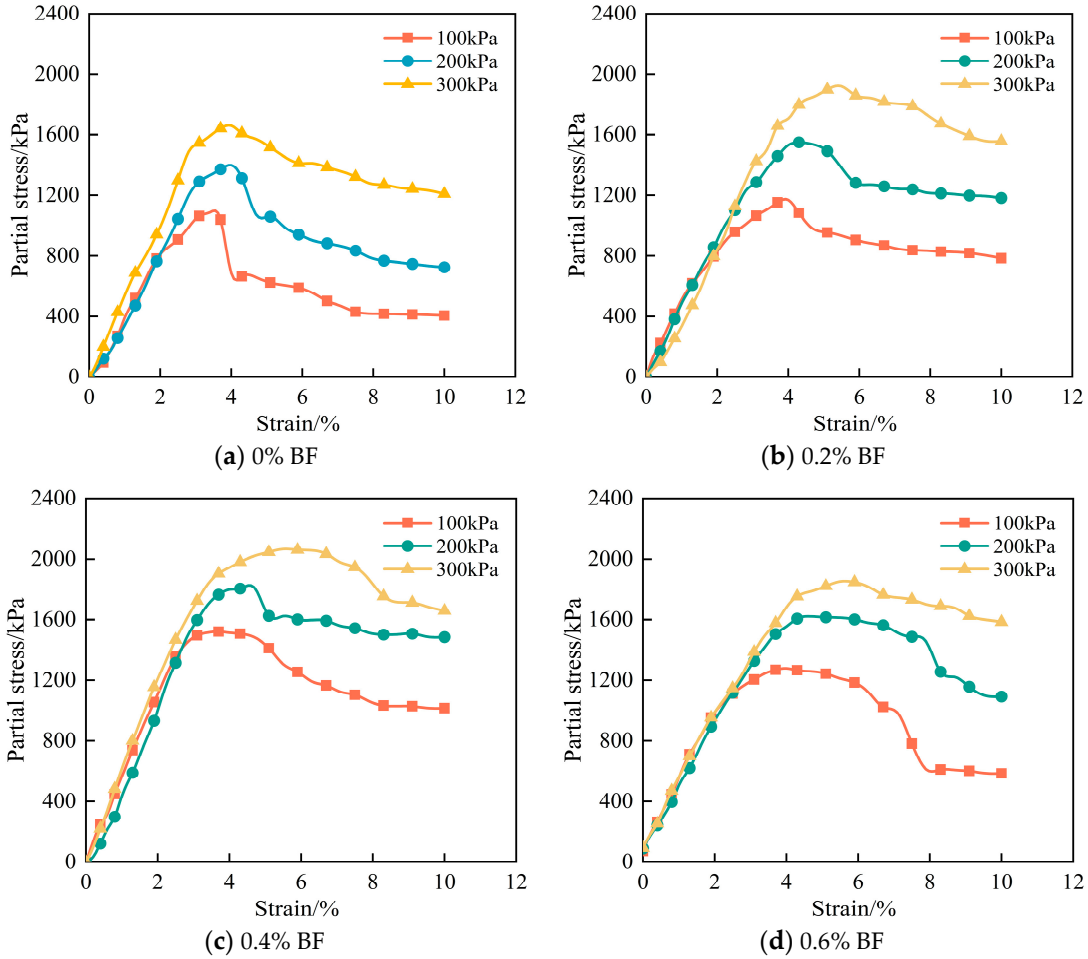

Figure 12. Partial stress–strain curves of cement-stabilized expansive soil at different BF contents under different perimeter pressures.

Following the addition of BF, the partial stress–strain curves of cement-stabilized expansive soil underwent significant changes, as depicted in Figure 12b,c. Upon comparison with Figure 12, it becomes apparent that the softening behavior of the cement-stabilized expansive soil was substantially diminished in the presence of BF. The softening phenomenon

observed after the soil stress reached its peak value subsequent to the addition of BF to the cement-stabilized expansive soil was markedly reduced. Furthermore, the strain required for the stabilized soil to reach its maximum fractional stress increased. Additionally, the specimens demonstrated the ability to maintain high residual strength after damage. This phenomenon underscores the efficacy of BF in enhancing the ductility of the soil, thereby compensating for the limitations of relying solely on cement to stabilize expansive soil.

3.3.3. Shear Strength

Calculating the shear strength of the cement-stabilized expansive soil helped in understanding the impact of BF content and perimeter pressure on the soil's resistance to shear forces. Figure 13 illustrates the shear strength of the cement-stabilized expansive soil at various BF contents under different perimeter pressures. As depicted in Figure 8, both the BF content and the magnitude of perimeter pressure exerted a significant influence on the shear strength of cement-stabilized expansive soil. The shear strength of the specimens initially rises and then declines with increasing BF content across all levels of perimeter pressure. This indicates that the addition of BF effectively enhanced the shear performance of cement-stabilized expansive soil. Notably, the shear strength exhibits a roughly linear increase as the BF content escalates from 0% to 0.4%. Conversely, a decrease in shear strength was observed with an increase in BF content from 0.4% to 0.6%. This phenomenon suggests that an addition of 0.4% BF yielded the most favorable improvement in shear strength for cement-stabilized expansive soil. The shear strength increased by 40%, 29.4%, and 24.6% at perimeter pressures of 100 kPa, 200 kPa, and 300 kPa, respectively.

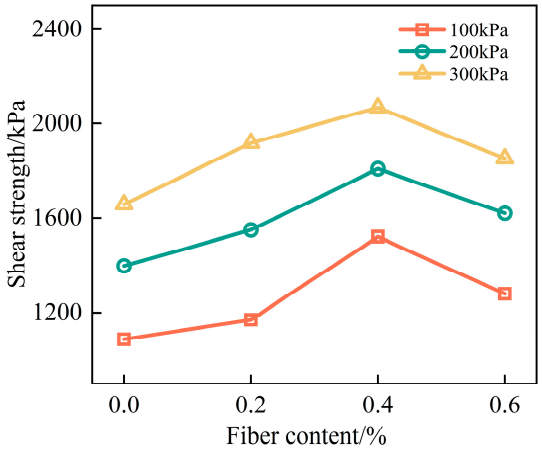

Figure 13. The shear strength of cement-stabilized expansive soil at different BF contents under different perimeter pressures.

3.3.4. Cohesion and Internal Friction Angle

Calculating the cohesion and internal friction angle helped in understanding how different BF contents affected the stability and shear strength of the cement-stabilized expansive soil, as these parameters are critical indicators of soil strength and resistance to deformation. The curves depicting cohesion and the angle of internal friction of cement-stabilized expansive soil at various BF contents are presented in Figure 14. As depicted in Figure 14, the cohesion of the cement-stabilized expansive soil increased when the BF content was below 0.4%. However, as the BF content continued to rise, the cohesion decreased. This suggests that the cohesion of cement-stabilized expansive soil reached its peak at a BF content of 0.4%, representing a 34.5% increase compared to cement-stabilized expansive soil alone. Conversely, the angle of internal friction was minimally affected by the BF content, with a variation of only about 1.8%. The combination of cement and BF in expansive soil effectively enhanced the soil's shear strength, primarily by increasing soil cohesion.

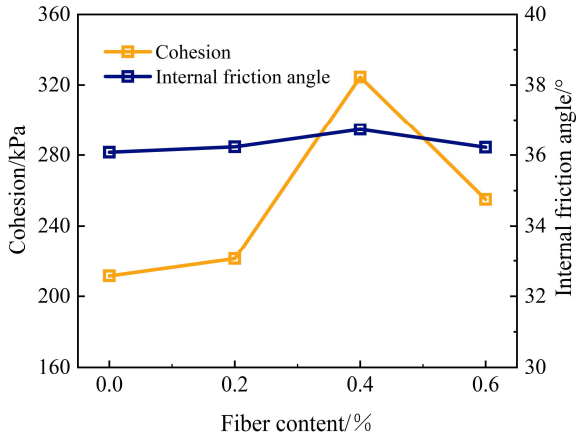

Figure 14. Cohesion and internal friction angle of cement-stabilized expansive soil at different BF contents.

3.4. Dry–Wet Cycle Durability

Since soils in nature frequently experience repeated dry–wet cycles, comprehending the variations in the UCS of enhanced expansive soils across different dry–wet cycles is critical for practical engineering applications. The UCS of cement-stabilized expansive soil at various BF contents under different dry–wet cycles is illustrated in Figure 15. Analysis of the figure revealed a two-stage change curve in the UCS of stabilized expansive soil under dry–wet cycles. The first stage, spanning from 0 to 3 dry–wet cycles, involved a rapid decline in specimen strength. The subsequent stage, encompassing 3 to 16 dry–wet cycles, further demonstrated the deteriorating effect of dry–wet cycles on UCS. The extent of degradation was closely linked to the number of dry–wet cycles. Specifically, the UCS of cement-stabilized expansive soil without BF decreased by 521 kPa after three dry–wet cycles, representing a 33.03% decrease. With the continued increase in the number of dry–wet cycles to 16, the UCS decreased by only 333 kPa, indicating a relatively minor decrease at this juncture.

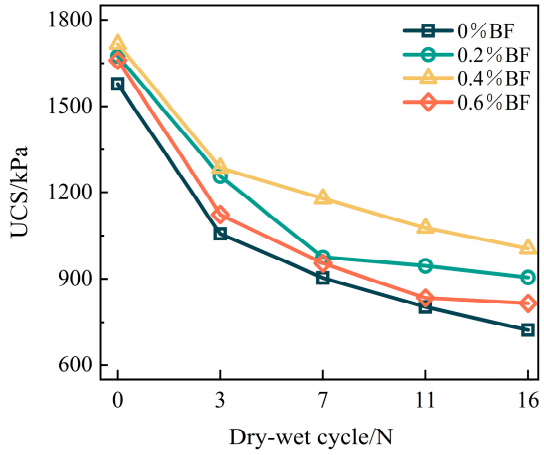

Figure 15. UCS of cement-stabilized expansive soil at different BF contents under different dry–wet cycles.

The incorporation of BF enhanced the resistance of cement-stabilized expansive soil to the cyclic effects of dry–wet conditions. As depicted in Figure 10, for a given number of dry–wet cycles, when the BF content was below 0.4%, the UCS of the cement-stabilized expansive soil increased gradually with the BF content. However, as the BF content increased from 0.4% to 0.6%, the UCS decreased. BF exhibits excellent tensile properties, and an optimal quantity of BFs creates a spatial reinforcement structure within a cement–soil composite. This structure effectively inhibits the formation of structural cracks and

enhances the UCS of a cement–soil mixture. However, increasing BF content reduces the workability of a cement–soil mixture, resulting in uneven BF distributions and diminished reinforcement effects. Consequently, the UCS of the cement–soil composite decreased with higher BF content. In essence, the UCS of the cement-stabilized expansive soil peaked when the BF content reached 0.4% under dry–wet cycles conditions. After 16 dry–wet cycles, the UCS of the specimens increased by 38.87% compared to specimens with cement-stabilized expansive soil. This suggests that moderate amounts of BF are beneficial in enhancing the resistance of cement-stabilized expansive soil to deterioration caused by dry–wet cycles.

To characterize the effect of BF on the durability performance of cement-stabilized expansive soil subjected to dry–wet cycles, the durability coefficient was defined as the ratio of the UCS of different specimens after the Nth dry–wet cycle to that of cement-stabilized expansive soil not subjected to dry–wet cycles:

$$D_N = \frac{q_i}{q_0} \tag{1}$$

In the equation, D_N represents the endurance coefficient after the Nth cycle; q_i denotes the UCS of the specimen after the Nth dry–wet cycle; and q_0 signifies the UCS of the cement-stabilized expansive soil that was not subjected to dry–wet cycles.

From the analysis in Figure 15, it is evident that the UCS decayed approximately exponentially with the number of dry–wet cycles and initially decreased with BF content. Therefore, a multivariate nonlinear fit was conducted using the number of dry–wet cycles and the BF blend as independent variables and the durability coefficient as the dependent variable, yielding the following relationship:

$$D_N = p_1 e^{p_2 N} + p_3 N + p_4 m^3 + p_5 m \tag{2}$$

In the equation, N represents the number of dry–wet cycles; m denotes the amount of BF; and p_1, p_2, p_3, p_4 and p_5 signify parameters.

The relationship equation for the durability coefficient in relation to the number of dry–wet cycles and BF content was derived through several iterative operations:

$$D_N = 0.9581\mathrm{e}^{-0.1334N} + 0.0234N - 1.431m^3 + 0.05995m \tag{3}$$

The correlation coefficient R = 0.98 indicates that the surface fit of the durability coefficient to the number of wet and dry cycles and BF content was satisfactory, as shown in Figure 16.

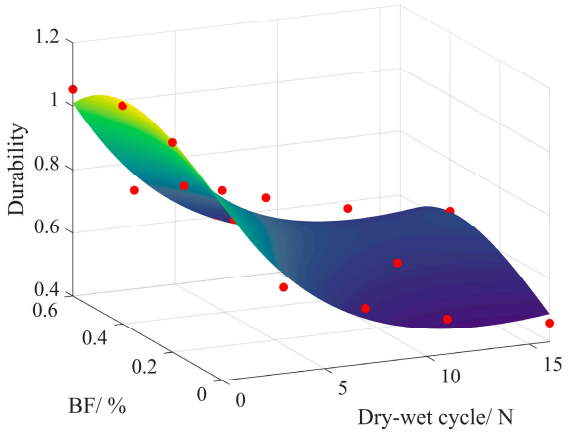

Figure 16. Surface fitting effect diagram of the relationship between durability, dry–wet cycle number, and BF dosage.

3.5. Microstructure

3.5.1. Microscopic Morphology and Mechanisms of BF Reinforcement

Figure 17 illustrates the interfacial interaction among the BF-expansive soil–gel product. As depicted in Figure 17, the gel product and expansive soil particles tightly adhered to the outer surface of the BF, facilitating the formation of a cemented interface and enhancing friction between them. This adherence created a potential sliding surface upon imminent damage to the specimen. A potential sliding surface was formed when the specimen was on the brink of damage. Both the BF and the soil particles experienced pressure simultaneously. However, due to their distinct material properties, they underwent different deformations, resulting in a tendency for misalignment between the BF and soil particles. Consequently, stress on the potential slip surface was transferred to the BF via interfacial forces between the BF and soil particles. Subsequently, when subjected to tension, BF dispersed stress around the soil via the potential slip surface. The failure or extraction of the BF diminished its role in distributing external loads and enhancing soil ductility. It is evident that the reinforcing effect of BF not only relied on the amount of frictional resistance and adhesion at the BF–soil contact interface but also on the tensile strength of the BF itself.

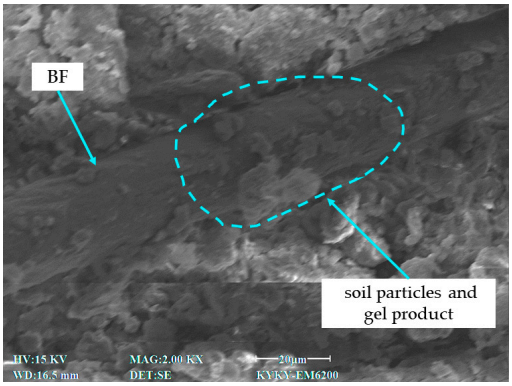

Figure 17. SEM image of the interfacial interaction between BF-expanded soil and gel products.

As per the principle of BF reinforcement discussed in the preceding section, it might have been theoretically inferred that a higher BF concentration in the soil would have enhanced the reinforcing effect of BF. However, the test results contradict this assumption. As illustrated in Figure 18a, when BF content was low, BF dispersed throughout the soil without forming connections with each other. Consequently, soil property enhancement relied solely on the independent reinforcing role of BF. Thus, BF exhibited a limited influence on the overall structure of the stabilized soil. Macroscopically, there was no significant increase observed in the UCS, shear strength, and cohesion of cement-stabilized expansive soil.

As the number of BF in the soil increased, it dispersed randomly and intertwined with itself. This enabled the formation of a fibrous network, as depicted in Figure 18b. When one BF was stretched, this necessitated the pulling of other BFs, forming a three-dimensional force network. This network allowed for the dispersion of loads over a broader area. The three-dimensional reinforcing effect of BF relied on the independent tensile effect of individual BFs [28]. Both reinforcement effects were influenced by the magnitude of interfacial forces between the BF and soil particles.

Mechanical tests indicated that the strength and cohesion of the specimens declined once the fibrous content surpassed 0.4%. Hence, an optimal BF content exists for reinforcing cement-stabilized expansive soil. As depicted in Figure 18c, surpassing this optimal value results in uneven BF distribution within soil, leading to cluster formation. This adversely impacts the filling effect of the gel product and creates weak interfaces within soil, ultimately diminishing soil's performance.

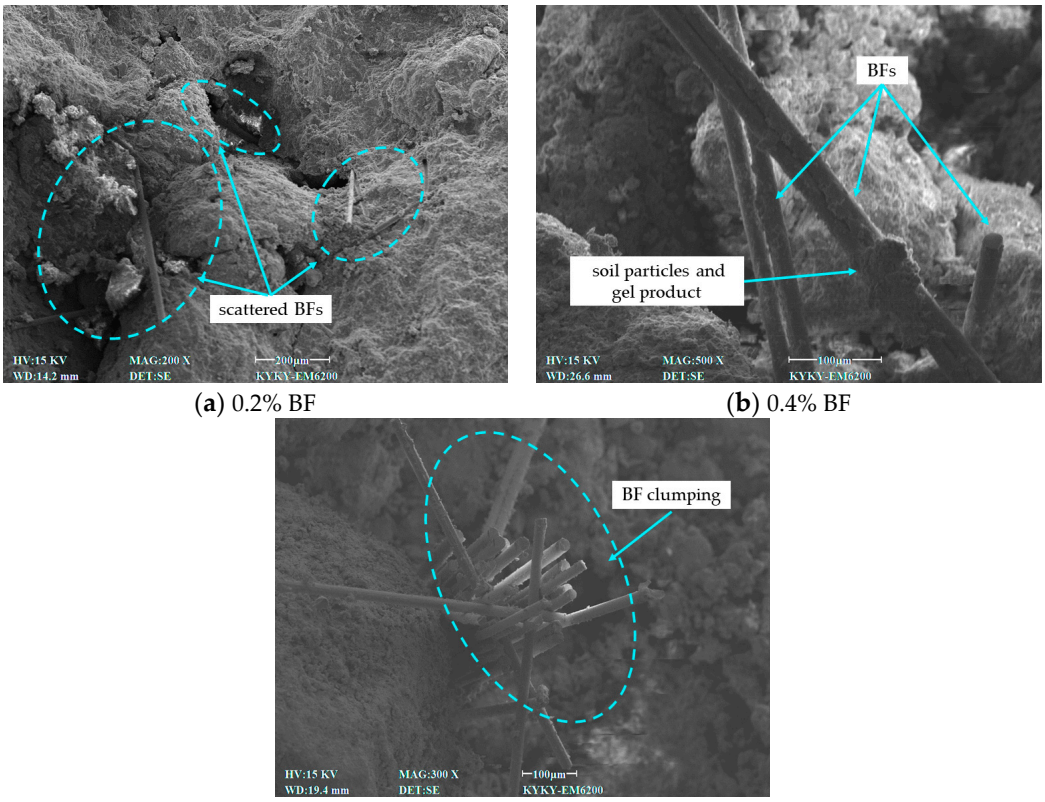

(**a**) 0.2% BF (**b**) 0.4% BF

(**c**) 0.6% BF

Figure 18. SEM images of microscopic BF distribution in expansive soil.

3.5.2. Microcosmic Mechanisms of Dry–Wet Cycle Deterioration

Figure 19 depicts the deterioration mechanism of the cement-stabilized expansive soils subjected to dry–wet cycles. With advancing curing age, cement-stabilized expansive soils underwent densification owing to the agglomeration and cement-filling effect of gel products, as illustrated in Figure 19. Expansive soils are rich in expansive clay minerals [29,30]. In the wetting phase of the dry–wet cycle, soil particles not enveloped by gel products absorb water, swell, and come into close contact with each other. During this phase, the cementing action of the gel product minimizes deformation caused by water absorption and soil particle swelling, consequently reducing the impact on the structural stability of expansive soil.

During the drying stage, two main phenomena occur. Firstly, the interparticle repulsive force diminishes as the adsorbed water on the soil particle surfaces evaporates, resulting in a reduction in interparticle distance. Secondly, the decrease in water content significantly amplifies matrix suction in the soil, exacerbating soil shrinkage. Consequently, the shrinkage of soil particles further enlarges the voids between agglomerates. When the matrix suction force surpasses the cementation force between agglomerates or soil particles, pores and microcracks form within the soil. Subsequently, these small pores progressively enlarge, eventually connecting to form larger pores. Once a critical number of large pores are established, they merge to create microcracks. These microcracks gradually expand and interconnect over successive dry–wet cycles. At a macroscopic level, this manifests as a reduction in mechanical strength.

According to the previous explanation, one reason for the deterioration of cement-stabilized expansive soil under dry–wet cycles is the breakdown of soil particles or aggregate cementation by the gel product. Another factor is the formation and propagation of microcracks. As illustrated in Figure 20, the random distribution of BF in the expansive soil allowed it to further impede crack expansion through a "bridging effect", resulting in a slower rate of water erosion. Consequently, the durability of cement-stabilized expan-

sive soil under dry–wet cycles is enhanced by the addition of BF. However, the original soil structure was somewhat compromised after experiencing dry–wet cycles, leading to relaxation and cracking at the interface between BF and soil particles. Consequently, the reinforcing effect of BF was weakened to some extent. Therefore, with an increasing number of dry–wet cycles, the strength of BF–cement-stabilized expansive soil still degrades, albeit to a lesser extent compared to cement-amended soil without fiber incorporation.

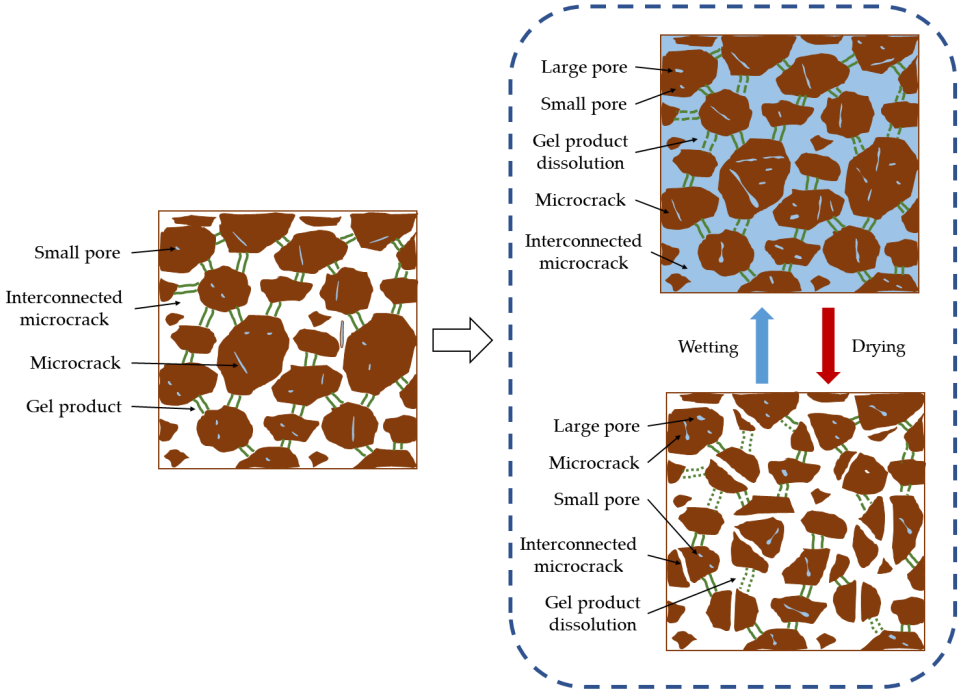

Figure 19. Deterioration mechanism of cement-stabilized expansive soil under dry–wet cycles.

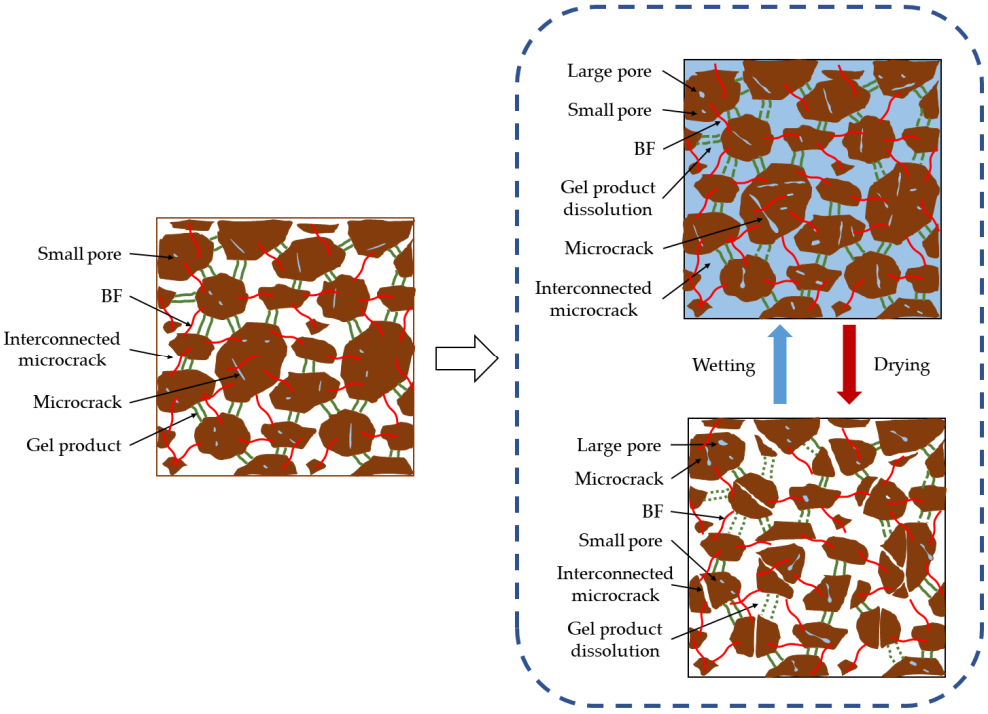

Figure 20. Deterioration mechanism of BF–cement-stabilized expansive soil under dry–wet cycles.

4. Conclusions

This study assessed the compaction, swelling, shrinkage, strength, and dry–wet cycle durability of cement-stabilized expansive soil enhanced by BF through geotechnical tests. Additionally, the enhancement mechanism of cement and BF stabilized expansive soil was analyzed via SEM testing, along with the deterioration mechanism during dry–wet cycles. The key findings are as follows.

1. The swelling, shrinkage, and strength properties of the soil initially increased and then decreased with increasing BF content. However, the maximum dry density remained unchanged. At the optimal BF content of 0.4%, swelling and shrinkage of the cement-stabilized expansive soil decreased by 36.17% and 28.4%, respectively. In terms of soil strength, BF was more effective in enhancing soil shear strength than compressive strength. The shear strength of cement-stabilized expansive soil with the addition of 0.4% BF increased by 24.8% to 40% at different perimeter pressures, while the compressive strength increased by 24.8%.

2. The effectiveness of BF in enhancing the performance of cement-stabilized expansive soil depends on the complexity of the network structure formed within the soil. A low content of BF results in limited reinforcement, as it relies on individual fibers. Optimal BF content, however, facilitates the formation of a reinforcing network, substantially enhancing soil cohesion. Conversely, excessive BF tends to cluster, creating structural weaknesses that hinder soil improvement.

3. Dry–wet cycles can cause degradation in the strength of cement-stabilized expansive soil. Initially, the soil strength declined significantly, with a more gradual decrease observed in later cycles. Following 16 dry–wet cycles, the UCS decreased by 54.15%. The ability of the cement-stabilized expansive soil to resist dry–wet cycles was enhanced by the incorporation of BF. Through the multivariate nonlinear regression analysis, the multivariate nonlinear equation of compressive strength of the cement-stabilized expansive soil on the number of dry–wet cycles and BF content was established, and the fitting effect was ideal. This is of some reference significance for the compressive strength projection of improved expansive soil under dry–wet cycles conditions in engineering.

4. SEM images showed that the strength degradation during the dry–wet cycle stemmed from the disruption of soil particle or aggregate cementation by the gel product, along with the ongoing development and expansion of microcracks in the specimens. The incorporation of BF enhanced the dry–wet cycle durability of the cement-stabilized expansive soil. During the dry–wet cycles, the UCS initially increased and then decreased with the addition of BF. Optimal durability performance was achieved at a BF content of 0.4%. After 16 dry–wet cycles, the UCS increased by 38.87% compared to the cement-stabilized expansive soil without BF. This is attributed to the random distribution of BF in the soil, which restricted cracking and reduced the rate of water erosion.

5. This study experimentally demonstrated the effectiveness of BFs in improving the swelling and shrinkage characteristics of cement-stabilized expansive soils, increasing soil strength, and enhancing resistance to dry–wet cycles. The findings suggest that fibers can replace some traditional cementitious materials for soil improvement, helping to reduce construction costs and promote sustainable development. While these results have significant economic and environmental benefits, they are only applicable to similar soils. Future research will focus on optimizing fiber–cement ratios and exploring a broader range of applications for diverse soil types to enhance the effectiveness and sustainability of engineering practices.

Author Contributions: Conceptualization, J.C.; methodology, J.M.; validation, A.C.; formal analysis, Y.Z.; investigation, J.Z.; resources, Y.L.; data curation, J.M.; writing—original draft preparation, J.M.; writing—review and editing, A.C. and Y.L.; supervision, J.C.; project administration, J.C. All authors have read and agreed to the published version of the manuscript.

Funding: (1) Junhua Chen; Science and Technology Base and Talent Special Project (GUIKE AD21220051). (2) Aijun Chen; Guangxi Natural Science Foundation Project (2022GXNSFAA035485). (3) Yao Long; Hunan Natural Science Foundation Sectoral Joint Fund (2024JJ8021). (4) Yao Long; Hunan Provincial Department of Education Scientific Research Project (22B0958).

Institutional Review Board Statement: Not applicable.

Informed Consent Statement: Not applicable.

Data Availability Statement: All data used in this study are contained within this paper.

Conflicts of Interest: The authors declare no conflicts of interest.

References

1. Liu, C.; Wu, Z.; Garg, A.; Qin, Y.; Mei, G.; Lv, C.; Zhang, H. Experimental investigation for dynamic propertys of paraffin-graphite based CPCM (composite phase change material) amended expansive soil under dry-wet cycles. *Constr. Build. Mater.* **2023**, *404*, 133170. [CrossRef]
2. Wu, Y.; Li, D.; Hu, X.; Han, T.; Yu, J.; Shi, K.; Wang, H.; Cao, Y. Experimental Study on Strength Propertys of Expansive Soil Improved by Steel Slag Powder and Cement Under Dry–Wet Cycles. *Iran. J. Sci. Technol. Trans. Civ. Eng.* **2020**, *45*, 941–952. [CrossRef]
3. Miao, L.; Wang, F.; Ye, W.-m.; Jiang, M.; Li, J.; Shi, S. Combined method limiting shrinkage–swelling behaviours of expansive soils in Huai'an, China. *Environ. Geotech.* **2021**, *8*, 334–344. [CrossRef]
4. Zhen, H.; Sun, H.-Y.; Dai, Y.-M.; Hou, P.-B.; Zhou, W.-Z.; Bian, L.-L. A study on the shear strength and dry-wet cracking behaviour of waste BF-reinforced expansive soil. *Case Stud. Constr. Mater.* **2022**, *16*, e01142.
5. He, P.; Li, S.-C.; Xiao, J.; Zhang, Q.-Q.; Xu, F.; Zhang, J. Shallow Sliding Failure Prediction Model of Expansive Soil Slope based on Gaussian Process Theory and Its Engineering Application. *KSCE J. Civ. Eng.* **2018**, *22*, 1709–1719. [CrossRef]
6. Rosenbalm, D.; Zapata, E.C. Effect of Wetting and Drying Cycles on the Behavior of Compacted Expansive Soils. *J. Mater. Civ. Eng.* **2016**, *29*, 04016191. [CrossRef]
7. Liu, C.; Lu, K.; Wu, Z.; Liu, X.; Garg, A.; Qin, Y.; Mei, G.; Lv, C. Expansive soil improvement using industrial bagasse and low-alkali ecological cement. *Constr. Build. Mater.* **2024**, *423*, 135806. [CrossRef]
8. Lu, Y.; Liu, S.; Zhang, Y.; Li, Z.; Xu, L. Freeze-thaw performance of a cement-treated expansive soil. *Cold Reg. Sci. Technol.* **2020**, *170*, 102926. [CrossRef]
9. Yan, J.; Li, T.; Kong, L.-W.; Luo, X.; Zhou, Z.; Wang, J. Nonlinear decay behavior of small strain dynamic shear modulus of lime-treated expansive soil. *J. Soils Sediments* **2023**, *23*, 3310–3325. [CrossRef]
10. Festugato, L.; Menger, E.; Benezra, F.; Kipper, E.A.E.; Consoli, N.C. BF-reinforced cemented soils compressive and tensile strength assessment as a function of filament length. *Geotext. Geomembr.* **2017**, *45*, 77–82. [CrossRef]
11. Yang, B.-H.; Weng, X.-Z.; Liu, J.-Z.; Kou, Y.-N.; Jiang, L.; Li, H.-L.; Yan, X.-C. Strength propertys of modified polypropylene fiber and cement-reinforced loess. *J. Cent. South Univ.* **2017**, *24*, 560–568. [CrossRef]
12. Tariq, M.W.; Israr, J.; Farooq, K.; Mujtaba, H. Strength Mechanism of a Swelling Soil Improved with Jute Fibers: A Laboratory Treatment. *Geotech. Geol. Eng.* **2023**, *41*, 4367–4380. [CrossRef]
13. Pourakbar, S.; Fasihnikoutalab, M.; Ball, R.; Cristelo, N.; Huat, B. Soil reinforcement through addition and subsequent carbonation of wollasonite microfibres. *Geosynth. Int.* **2017**, *24*, 554–564. [CrossRef]
14. Kanchi, G.M.; Neeraja, V.S.; Babu, G.L.S. Effect of Anisotropy of Fibers on the Stress-Strain Response of Fiber-Reinforced Soil. *Int. J. Geomech.* **2014**, *15*, 06014016. [CrossRef]
15. Adhikari, B.; Khattak, M.J.; Adhikari, S. Mechanical and durability propertys of flyash-based soil-geopolymer mixtures for pavement base and subbase layers. *Int. J. Pavement Eng.* **2021**, *22*, 1193–1212. [CrossRef]
16. Abdullah, H.H.; Shahin, A.M.; Sarker, P. Use of Fly-Ash Geopolymer Incorporating Ground Granulated Slag for Stabilisation of Kaolin Clay Cured at Ambient Temperature. *Geotech. Geol. Eng.* **2019**, *37*, 721–740. [CrossRef]
17. Chowdary, V.B.; Ramanamurty, V.; Pillai, R.J. Experimental evaluation of strength and durability propertys of geopolymer stabilised soft soil for deep mixing applications. *Innov. Infrastruct. Solut.* **2020**, *6*, 40. [CrossRef]
18. Zhang, H.; Liu, T.; Cui, Y.; Wang, Z.; Wang, W.; Zheng, J. Compression and shear properties of OPC-MCA and basalt fiber cured shield waste mud after dry-wet cycles. *Constr. Build. Mater.* **2024**, *426*, 136153. [CrossRef]
19. Shu, H.; Yu, Q.; Niu, C.; Sun, D.; Wang, Q. The coupling effects of wet-dry and freeze–thaw cycles on the mechanical properties of saline soil synergistically solidified with sulfur-free lignin, basalt fiber and hydrophobic polymer. *Catena* **2024**, *238*, 107832. [CrossRef]
20. Nguyen, L.; Fatahi, B. Behaviour of clay treated with cement & fibre while capturing cementation degradation and fibre failure—C3F Model. *Int. J. Plast.* **2016**, *81*, 168–195.
21. Xu, Y.; Han, Y.; Zhao, G.; Meng, S. Enhancing geotechnical reinforcement: Exploring molybdenum tailings and basalt BF-modified composites for sustainable construction. *Constr. Build. Mater.* **2024**, *411*, 134452. [CrossRef]
22. Ralegaonkar, R.; Gavali, H.; Aswath, P.; Abolmaali, S. Application of chopped basalt fibers in reinforced mortar: A review. *Constr. Build. Mater.* **2018**, *164*, 589–602. [CrossRef]

23. Xue, G.; Liang, H.; Pu, Y.; Wang, D.; Wang, Y. Enhancing thermal stability and tensile performance of short basalt fiber-reinforced PLA composites with PBAT and nano-silica. *Compos. Commun.* **2024**, *48*, 101894. [CrossRef]
24. Chen, Z.; Wang, X.; Ding, L.; Jiang, K.; Su, C.; Ben, Q.; Wu, Z. Effects of macro basalt fibers on the tensile behavior of ultra-high performance concrete. *J. Build. Eng.* **2024**, *89*, 109277. [CrossRef]
25. Sun, Z.; Kou, C.; Lu, Y.; Wu, Z.; Kang, A.; Xiao, P. A Study of the Bond Strength and Mechanism between Basalt Fibers and Asphalt Binders. *Appl. Sci.* **2024**, *14*, 2471. [CrossRef]
26. *GB/T 50123*; Geotechnical Test Standard. Ministry of Housing and Urban-Rural Development of the People's Republic of China: Beijing, China, 2019.
27. *GB 50112*; Technical Code for Building in Expansive Soil Region. Ministry of Housing and Urban-Rural Development of the People's Republic of China: Beijing, China, 2013.
28. Ibraim, E.; Camenen, J.; Diambra, A.; Kairelis, K.; Visockaite, L.; Consoli, N.C. Energy efficiency of BF reinforced soil formation at small element scale: Laboratory and numerical investigation. *Geotext. Geomembr.* **2018**, *46*, 497–510. [CrossRef]
29. Dai, Z.; Huang, K.; Chi, Z.; Chen, S. Model test study on the deformation and stability of rainfall-induced expansive soil slope with weak interlayer. *Bull. Eng. Geol. Environ.* **2024**, *83*, 76. [CrossRef]
30. Chang, J.; Xu, Y.-F.; Xiao, J.; Wang, L.; Jiang, J.-Q.; Guo, J.-X. Influence of acid rain climate environment on deterioration of shear strength parameters of natural residual expansive soil. *Transp. Geotech.* **2023**, *42*, 101017. [CrossRef]